Performance enhancement and scaling control with gas bubbling in a direct contact membrane distillation

Chen, Guizi; Wang, Rong; Fane, Anthony Gordon; Yang, Xing

2012

Chen, G. Z., Yang, X., Wang, X., & Fane, A. G. (2013). Performance enhancement and scaling control with gas bubbling in a direct contact membrane distillation. Desalination, 308, 47-55.

https://hdl.handle.net/10356/102150

https://doi.org/10.1016/j.desal.2012.07.018

Performance enhancement and scaling control with gas bubbling in direct contact membrane distillation

Guizi Chen, Xing Yang, Rong Wang*, Anthony G. Fane

School of Civil and Environmental Engineering, Nanyang Technological University, Singapore 639798

Singapore Membrane Technology Centre, Nanyang Technological University, Singapore 639798

*Corresponding author at: School of Civil and Environmental Engineering, Nanyang Technological University, 639798 Singapore

Singapore. Tel.: +65 6790 5327; fax: +65 6791 0676.

E-mail address: rwang@ntu.edu.sg (R. Wang).

Abstract

This study incorporates gas bubbling into direct contact membrane distillation (DCMD) and examines its effect on the MD performance especially at elevated salt concentrations in the feed steam. Process optimization in the bubbling assisted DCMD process was carried out which involved varying operating conditions and module configurations. Also, observations were performed for the scaling status on the membrane surface with operating time in different modules to further understand the role of gas bubbling in affecting the behavior of crystal deposition when the salt concentration has reached super-saturation.

Due to intensified local mixing and physical flow disturbance in the liquid boundary layer on the feed side, a higher flux enhancement could be achieved in a bubbling system with either a higher feed operating temperature, lower feed and permeate flow velocities, inclined module orientation, shorter fiber length or lower packing density. It was also found that gas bubbling not only enhanced the permeation flux by average 26% when concentrating feed solution from 18% salt concentration to saturation, but also delayed the occurrence of major flux decline due to crystal deposition when compared to the module with spacers. These results were confirmed by membrane surface autopsy at different operating stages SEM.

Keywords: membrane distillation; high salt concentration; gas bubbling; flux enhancement ratio; scaling.

1. Introduction

Membrane distillation (MD) is well recognized as a potential alternative technology for desalination due to the benefits of moderate operating temperature with acceptable permeation rate, high salt rejection and low greenhouse gas emissions when operated with available low-grade waste heat [1-5]. Importantly, MD has an attractive advantage over other desalination processes (e.g. reverse osmosis (RO)), which is that the elevated salt concentration in the feed stream has a smaller impact on the mass flux [5,6].

However, one of the major barriers in MD applications is the decrease of driving force due to concentration and temperature polarization phenomena [7-11]. In addition, if the salt concentration in the feed is close to the super-saturation, the evaporation at the membrane pores could lead to salt crystals being formed and deposited on the membrane surface, leading to a dramatic flux decline because of the blockage of water transport passage [6]. Therefore, in order to prevent the decrease of water permeation and prolong membrane life in a high concentration MD process, the surface shear near membrane surface needs to be increased [12,13]. Gas bubbling is one of effective ways to enhance the surface shear rate for fouling control. The introduction of a gas-liquid two-phase flow has significantly enhanced the performance of several membrane processes [14].For example, the use of gas bubbling to create better fluid dynamics to control external fouling, was proposed by Tajima and Yamamoto in 1988 [15]. In the 1990s, a number of studies demonstrated that creating a

gas-liquid two-phase flow at the feed side was an effective method to limit membrane fouling, with the trans-membrane flux being increased significantly [16-18]. Extensive studies since 2000 also revealed that bubbling-induced secondary flows greatly increased the maximum shear stress near the membrane surface, thus the foulant deposition was constrained [19-23]. Most importantly, when correctly used gas bubbles impose less risk of membrane damage and can be easily separated from the main process stream [14].

To date the use of bubbling with MD has been limited to the studies on the MD bioreactor [24]. To our knowledge, no prior work on MD for high concentration applications has systematically studied gas bubbling to mitigate concentration and/or temperature polarization effects and control crystal deposition and scaling formation. The aim of the current work is to explore the potential of gas bubbling in the MD process using direct contact MD (DCMD) with hollow fibers especially with elevated salt concentrations in the feed stream.

2. Theory and methodology

2.1 Mass and heat transfer analysis in DCMD

In a membrane separation process, the permeation flux J can be calculated from experimental parameters (i.e. the mass of the permeate, the effective membrane area and time interval taken). Also, J can be determined theoretically by the product of the overall mass transfer coefficient and the 'average' transmembrane vapor pressure difference [25].

Due to the presence of the concentration and temperature polarization phenomena in DCMD, the wall concentrations and temperatures can be significantly different from the bulk phase. In the heat and mass transfer processes of MD, temperature polarization can affect the driving force significantly, while concentration polarization may affect the MD performance only when the feed concentration is close to the salt saturation [8,26].

To assess the heat-transfer efficiency in DCMD, the membrane wall temperatures can be estimated from the inlet and outlet diameters of the membrane fibers, the heat-transfer coefficient of the membrane, the heat transfer coefficient associated with vapor flow, and the film heat-transfer coefficients of the feed and permeate sides, which can be expressed in terms of the Nusselt number (*Nu*). And the Nu_i is correlated with the Reynolds number, Prandtl number and Graetz number. The shell-side Nu_f can be obtained via Short's equation [27]:

$$Nu_f = 0.16 \times {R_{ef}}^{0.6} \times {P_{rf}}^{0.33} \times (\mu_f/\mu_{wf}\ )^{0.14} \qquad (200 \leq R_{ef} \leq 20000) \tag{1}$$

Meanwhile, the tube-side Nu_p can be calculated based on the Hausen's (Eq. (2)) or the Sieder-Tate's equation (Eq. (3)) [28] under the respective conditions:

$$Nu_p = 3.66 + \frac{0.19{Gz_p}^{0.8}}{1+0.1117{Gz_p}^{0.467}}(\frac{\mu_p}{\mu_{Wp}})^{0.14} \qquad (0.1 \leq Gz_p \leq 100) \tag{2}$$

$$Nu_p = 1.86 + {Gz_p}^{0.33}(\frac{\mu_p}{\mu_{Wp}})^{0.14} \qquad (Gz_p > 100) \tag{3}$$

where L is the fiber length, m, μ_f and μ_p are the viscosity at the bulk fluid temperature of the feed and permeate, and μ_{Wf} and μ_{Wp} are the viscosity at the heat-transfer boundary surface temperature of the feed and permeate, Pa·s.

To evaluate the effect of temperature polarization phenomenon in MD, the temperature polarization coefficient (*TPC*) is defined as the deviation of the transmembrane temperature difference from the bulk temperature difference [10,29]. As a major cause of trans-membrane driving force reduction, the temperature polarization phenomenon could result in significant flux decline in MD.

2.2 Flux decline in a high concentration DCMD

As mentioned previously, the MD performance will be greatly affected by the temperature polarization due to the relationship between the vapour pressure and the temperature at the membrane surface. Also, the vapour pressure difference (driving force) is modestly influenced by the solute content when the concentration goes up to a certain level. In general, an increase in the concentration will lead to a flux decline, which is due to the reduction of vapour pressure in feed side.

Therefore, in a batch MD operation without feed supplement, a gradual increase in salt concentration of the feed solution will result in a gradual flux decline before a critical level of saturation. Once a certain super-saturation of feed solution reached adjacent to the membrane surface, crystals would deposit on membrane surface and a dramatic flux decline would occur due to decrease the permeability of membrane fibers.

3. Experimental

3.1 Material properties and MD module specifications

As described in our previous work [26], a polyvinylidene fluoride (PVDF) hollow fiber MD membrane made by a commercial supplier was used to fabricate MD modules. Relevant membrane properties were characterized and are reported in Table 1. Dynamic contact angle was measured by a tensiometer (DCAT11 Dataphysics, Germany), the mechanical strength was tested by a Zwick 0.5 kN Universal Testing Machine at room temperature and the pore size distribution were determined by a capillary flow porometer (model CFP 1500A, from Porous Material. Inc.). More information on the methodologies for MD membrane characterization can be found elsewhere [13,26]. It can be seen that this highly porous PVDF fiber showed reasonably high liquid entry pressure for water (LEPw), good mechanical strength, small maximum pore size and a narrow pore-size distribution.

Table 2 lists the specifications of the membrane modules prepared with two different sizes of Teflon housings. Module #1 (d_s =6 mm) was packed with hollow fibers for flux assessment, the fiber length ranges from 210 to 480 mm and packing density from 8% to 49% for the configuration study; while modules #2 and #3 (inserted with spacer-knitted fibers, as shown in Figure 1 (a)-(b)) have the same d_s of 9.5 mm and were used for scaling observation. The fabrication details of module #3 can be found in our previous work [26].

Four different flow patterns (displayed in Figure 1(c)) were used to investigate the effect of module orientation in the presence of gas bubbling in a 340 mm long module, which included the modes of 45° inclined flow, horizontal flow, vertical up-flow of feed and vertical down-flow of feed. For all other experiments, the mode of vertical up-flow of feed was adopted.

3.2 Bubble-assisted DCMD process set up

The DCMD equipment was similar to our previous work [13,26]. The bulk temperatures were measured by thermocouples connected to data acquisition and the flow rates were monitored by in-line digital flow meters. The water flux was measured as weight gain in the cool permeate reservoir and recorded every thirty minutes. The feed solution was heated by a heating bath (Polyscience® 9105) and the temperature of the permeate reservoir was kept constant using a cooler (Julabo® F25). The feed and permeate were circulated counter-currently using a peristaltic pump (Masterflex®, Cole Palmer). Furthermore, gas bubbling is supplied by an air pump. The air inlet at the feed side entrance of the membrane module and the air nozzle for dispersing the air are shown in Figure 2.

3.3 Experimental procedure and error assessment

The DCMD experiments were run using similar procedures described elsewhere [26]. Both

the feed and permeate solutions were cycled through the hollow fibre module in countercurrent mode. On the shell side, the liquid feed (sodium chloride solution) was heated (in the range of 313-340 K) and circulated by a peristaltic pump (0.1-1 $L \cdot min^{-1}$). On the lumen side, the permeate side (DI water) was cooled down by a cooling circulator and cycled by another peristaltic pump (0.01-0.05 $L \cdot min^{-1}$). The distillate was collected in an overflow tank sitting on a balance (±0.1 g). Subsequently, the set of experiments were repeated with bubbling using the same membrane module. At the inlet of the membrane module, the gas flow from the air pump was added and mixed with the liquid feed, so that a two-phase flow passed over the membrane surface of the feed side.

For experiments involving crystal deposition, the DCMD system was run separately for a specified time using different modules. After high concentration DCMD experiments, the membrane modules were dismantled immediately for autopsy. The fouled hollow fibres taken from the module were cut carefully to remain the depositing crystals on the membrane. Membrane cross section and surface with nondestructive crystals were selected and made for SEM (Scanning Electron Microscope) samples. These SEM samples were then dried in the vacuum drying oven. After 12 hours, the status of scaling and crystal deposition on the samples was investigated using SEM.

To characterize the performance improvement achieved by gas bubbling, the flux enhancement ratio Φ is defined as:

$$\Phi = \frac{J_{gas}}{J_{nogas}} \quad (4)$$

where J_{gas} and J_{nogas} are the permeate fluxes in the DCMD process with and without bubbling, respectively.

All the experiments were repeated and showed good reproducibility with water fluxes within ±8% (illustrated as error bars in the figures). The conductivity meter had an accuracy of ±0.1 ms·cm^{-1} (feed side) and ±0.1 μs·cm^{-1} (permeate side), respectively. The temperature and flow rate variations were strictly controlled within ±0.4 °C and ±0.01 L·min^{-1}, respectively.

4. Results and discussion

4.1 Process optimization in bubbling assisted DCMD process

4.1.1 Effect of feed temperature

In the MD process, the operating temperature is an essential parameter as the driving force increases exponentially with increasing temperature. Figure 3 shows the flux enhancement ratio Φ as a function of the feed temperature. It can be seen that the water flux has increased considerably ($\Phi > 1$), which indicates that the introduction of gas bubbles has enhanced the permeation rate compared to a non-bubbling system. The enhancement may be due to the fiber movement and enhanced mixing caused by the flowing bubbles. With the flow disturbance by bubbling, the thermal boundary layer in the feed side may be reduced, leading

to an increase of the trans-membrane temperature difference (driving force). As a result, the permeation rate increases significantly with the aid of bubbles.

In addition, it is observed that Φ increases with increasing feed temperature T_f from 1.18 (at T_f = 313 K) to 1.43 (at T_f = 340 K). This tendency illustrates that gas bubbling tends to be more effective in a higher temperature of the feed side, which can be explained by the *TPC* results shown in Figure 3. It can be seen that the *TPC* decreases from 0.93 to 0.65 with increasing feed temperature from 313 K to 340 K in a DCMD system without bubbling. This decreasing trend is due to a more significant decrease of the membrane wall temperature on the feed side, T_{fm}, induced by the higher evaporation rate at a higher temperature, and a rapid increase of the wall temperature at the permeate T_{pm} caused by the condensation of a larger amount of vapor. As a result, a lower trans-membrane temperature difference (T_{fm} - T_{pm}) and hence a smaller *TPC* occur at a higher operating temperature. Thus, a more effective role of gas bubbling and a higher Φ value could be obtained at a higher operating temperature.

4.1.2 Effect of hydrodynamic conditions

Besides the operating temperature, another essential aspect in MD is the hydrodynamic conditions, which are associated with the feed, permeate and gas flow velocities in a bubbling-assisted DCMD system. Experiments studied the effects of gas flow rate and liquid flow velocities (characterized as Reynolds numbers, *Re*, of the feed and permeate) on the flux

enhancement induced by the gas bubbling.

4.1.2.1 Gas flow rate under laminar and turbulent conditions. Figure 4 shows the effect of gas flow rate on the flux enhancement ratio Φ under laminar (Re_f = 842) and turbulent (Re_f = 2808) flows (based on liquid flows), respectively. It is observed that these two Φ curves present a similar trend, i.e., the Φ initially increases with increasing gas flow rate (corresponding to a range of $0 \leq Q_g \leq 0.2$ L·min^{-1} for the laminar flow and $0 \leq Q_g \leq 0.5$ L·min^{-1} for the turbulent flow, respectively) and then decreases at higher gas rates. The reason for the increase may be due to the fiber movement and secondary flows induced by the flow of gas bubbles, which effectively disrupts the boundary layer and promotes local mixing near the membrane surface. Hence, the mass and heat transfer processes have been significantly intensified. However, the Φ value decreases from 1.54 to 1.26 for the laminar condition and from 1.20 to 1.07 for the turbulent flow with a further increase of gas flow rate. This may be because that the amplitude of membrane movement had reached a plateau value, and large bubbles or slugs in the feed side led to local by-passing and a lower temperatures on the feed side. Also, an unreasonably high gas flow rate might increase energy consumption and result in potential damage of the fibers. Therefore, it is necessary to identify an optimal range of gas flow rates that are able to contribute to significant enhancements of mass and heat transfer.

Furthermore, Figure 4 shows that the Φ value of the laminar condition is much higher than that of the turbulent flow with the other operating parameters kept constant. That is due to a

thicker liquid boundary layer is apt to form and more severe temperature and concentration polarization phenomena easily occur at laminar conditions compared to a turbulent flow, where local mixing is already intensified and boundary layer is minimized. Hence, the introduction of gas bubbles is more helpful for a laminar flow, due to the improved flow conditions and increased transmembrane driving force with a reduced boundary layer.

4.1.2.2 Flow velocities of the feed and permeate. Figure 5 presents the flux ratio Φ as a function of the liquid feed flow velocity (Re_f) at a fixed gas flow rate Q_g = 0.2 L·min^{-1} and fixed Reynolds number of the permeate side Re_p = 552. The results show that the Φ value decreases dramatically from 1.72 to 1.18 at a relatively low Re_f ranging from 280 to 1400. However, a fairly insignificant decrease is observed at a higher Re_f range of 1400 to 2808. The significant flux enhancement at a lower flow velocity (Re_f) could be due to an effective fiber movement and the formation of intensive vortices caused by the bubbles, which induce local mixing and surface renewal to enhance mass and heat transfer. The decrease of the enhancement ratio Φ is probably because the original liquid boundary layer has already been effectively reduced at a high flow velocity, so that the trans-membrane temperature difference (driving force) is not much affected by the introduction of gas bubbles. Moreover, the resistance of fiber movement at a higher Re_f is higher. In this case, the introduction of gas bubbles might not be an ideal option for flux enhancement. This observation is consistent with that of Figure 4.

Experiments were also conducted to investigate the effect of permeate flow velocity (Re_p) in

the lumen on the flux enhancement ratio Φ. Figure 6 plots the Φ value as a function of the Re_p (350 − 1200) under the same gas flow rate (Q_g = 0.2 L·min^{-1}) and a fixed Reynolds number in the feed side (Re_f = 842, laminar flow). Similar to that in Figure 5, the Φ value decreases with increasing Re_p. The reason may be due to increased resistance for fiber movement when the permeate flow velocity increases and hence the amplitude of fiber movement induced by gas bubbling reduces. Therefore, the local mixing adjacent to the feed-side membrane surface becomes less intensive and consequently a lower flux enhancement ratio Φ is obtained at a higher permeate velocity.

Based on the discussions of Figures 5 and 6, lower feed and permeate flow velocities are preferable for a bubbling-assisted DCMD system, in which the local mixing near the membrane surface is intensified and the boundary layer in the feed side is disturbed physically, and hence the driving force is maximized.

4.2 Influence of module configuration with bubbling

In a bubbling system, module configuration is an important element for the process design. Under the same operating conditions, experiments were performed to study the effects of module orientation, fiber length and packing density on the flux enhancement with the aids of gas bubbling.

4.2.1 Hollow fiber module orientation

Figure 7 shows the comparison of the flux enhancement ratios Φ obtained by four different module orientations in the presence of gas bubbling− 45° inclined, vertical up-flow of feed, vertical down-flow of feed and horizontal flow. With other operating parameters kept constant, the highest Φ value of 1.34 is achieved by the module with inclined 45˚ angle, followed by the vertical up-flow (Φ=1.28). The horizontal orientation gains the least enhancement (Φ=1.12). This is probably because the gas slugs in an inclined tube move faster than in a vertical and horizontal tube, which shows the smallest Φ value. The horizontal mode could also experience by-passing due to gas buoyancy. Interestingly, the vertical module with an upward flow performs better than that with downward flow. It may be attributed to a longer retention time of gas bubbling in the vertical module with an upward flow than that in vertical downward flow module.

4.2.2 Module length and packing density

The relationship between the flux enhancement ratio Φ and the fiber length is plotted in Figure 8, which shows that the Φ value decreases with increasing module length. This may be because the gas bubbles break and merge as they arise from the bottom. Therefore, the bubble size increases and the total number of bubbles decreases significantly along the fibers. As a result, the flux enhancement from gas bubbles is weakened as the module length increases.

The relationship between the overall mass transfer coefficient, *C*, and the fiber length is also plotted in Figure 8. The *C* value was calculated from the permeation flux dividing by the log-mean vapor pressure difference for the different length modules. Similarly, the *C* value curve shows a decreasing trend with increasing module length [26]. In other words, the driving force (trans-membrane temperature difference) decreases with increasing the length of the modules, which is consistent with the trend of the Φ curve. Overall, a reasonably short hollow fiber module is preferable for a higher enhancement ratio and *C* value in the bubbling MD process.

To further explore the effect of gas bubbles in different module configurations, Figure 9 shows the flux enhancement ratio Φ and global mass transfer coefficient *C* as a function of module packing density. The experimental results reveal that the Φ value decreases with increasing packing density. That is probably due to the Reynolds number in a loosely packed module is lower than that of a tightly packed configuration under the same feed flow rate. The better turbulent effect caused by gas bubbling appears at a relative lower Reynolds number than a non-bubbling system, which is consistent with the result of Figure 5. The global mass transfer coefficient *C*, as shown in Figure 9, decreases as the module packing density increases (similar results obtained in [26]). This result indicates the driving force (T_{fm} - T_{pm}) decreases with increasing packing density in a MD module, as bubbles break and disappear more easily in modules packed with more fibers. Hence, better performance (higher Φ and *C*

values) was attained in a loosely packed module. Based on the above discussion, a higher flux enhancement ratio Φ can be achieved using a hollow fiber module with an inclined orientation, shorter fibers and a lower packing density.

4.3 Scaling control in a high concentration DCMD process

Although MD is resilient in treating high concentration brines, a rapid flux decline has been reported [6], due to the crystal deposition and scaling formation on the membrane surface in a high concentration MD system. To investigate approaches for scaling mitigation in the high concentration DCMD process, experiments were carried out using three MD systems, which involve the original modules with and without bubbling as well as a modified module with spacers, respectively. The results are compared in Figure 10, which shows the trends of permeation flux and NaCl mass fraction of the effluent with operation time.

For the permeation flux, all curves under different conditions show a general decreasing trend with increasing operation time — a slow initial decrease followed by a dramatic major decline. The initial decrease is due to an increase of salt concentration and hence a slight decrease of vapor pressure difference across the membrane. It can be seen that none of the NaCl mass fractions at the outlet of the feed is higher than 27% (saturation concentration at 333 K) for the three modules. However, due to the concentration polarization and salt accumulation on the membrane surface with time, the salt concentration on the membrane surface may be over

the critical saturation point, resulting in salt crystal formation and deposition on the membrane surface. Consequently, a significant flux decline occurred, as observed in earlier studies [6].

In the initial stage, the module with spacers performs the best, followed by the original module with bubbling; while the non-bubbling original module has the lowest flux. However, a dramatic flux decline occurs to the module with spacers after 5-hour operation; while both the original modules with and without gas bubbling show prolonged critical points at the 7^{th} hour. The mass fraction of NaCl at which flux starts to rapidly decline is about 0.225 for the spacer module and > 0.23 for the other two modules. An earlier occurrence of the critical point for the module with spacers is probably due to the presence of insertions, which tend to retain NaCl crystals on the membrane surface after saturation. With the presence of gas bubbles, although the frequency of crystal collision is increased due to a decreased physical volume of the feed solution, the moving bubbles are still able to enhance the surface shear rate and clean the membrane surface to some extent. Therefore, the original membrane modules with and without bubbling show similar critical points of super-saturation. However, the membrane module with spacers has a disadvantage in the high concentration MD process.

To associate the flux decline phenomenon with the tendency of crystal deposition and/or scaling formation on the membrane surface, the membrane surfaces of the high concentration systems presented in Figure 10 were examined using SEM. Figure 11 shows the SEM pictures

of the cross-sections and surfaces of the membranes in the three MD systems after 1-hour, 5-hour and 7-hour operation, respectively. In Figure 11 (a), no crystal deposition is observed from the cross sections or surfaces of the membrane in any of the modules after 1-hour operation. Figure 11(b) shows the SEM images of the membrane surfaces and cross sections after 5-hour operation. Consistent with the flux results presented in Figure 10, the surface of the module with spacers is almost completely covered with NaCl crystals; while the original modules only have a relatively small amount of crystals formed, and the membranes used in the bubbling system shows the least deposition. This set of SEM pictures explains why a drastic flux decline occurs to the module with spacers after the fifth hour and a relatively slow decrease for the original modules. Taking the bubbling module as an example, the thin film induced by the slug flow can help to isolate the membrane wall from the super saturated salt solution at the liquid boundary layer. Hence, scaling formation on the membrane surface is postponed and heat transfer is enhanced under a high shear region created by the bubble flow.

After 7 hours of operation (Figure 11(c)), complete crystal coverage on the membrane surfaces for all the systems is observed. Again, this confirms the major flux decline in Figure 10, which shows a similar critical point at the seventh hour for the original modules with and without bubbling. Clearly, the corresponding flux decline of different systems is closely related to the status of scale formation on the membrane surfaces. A loss in membrane permeability is unavoidable as the crystals start growing. It can be concluded that the modified module with spacers is the most vulnerable to severe salt deposition within a short

period of time; while bubbling can help to prolong the effective operating time with a higher permeation flux and delay the critical point for major flux decline. More importantly, it can illustrate that the module with bubbling can dispose such high concentration of feed solution, while the modified module with spacers cannot do it. However, from an applications point of view, operations close to saturation increase the risk of crystal formation and scaling.

5. Conclusions

From this study, it was found that in a bubbling assisted DCMD module, the permeate flux enhancement ratio could reach up to 1.72 at an optimized gas flow rate. A higher flux enhancement ratio could be achieved at either a high feed operating temperature, low feed and permeate Reynolds numbers and a module with 45° inclined orientation, shorter fiber length or lower packing density. In all of these conditions the improved hydrodynamics due to bubbling could reduce temperature polarization. However it is observed that beyond an optimal gas flow the enhancement ratio falls, possibly due to excessive flow by-passing.

Compared to a modified module with spacers, the introduction of gas bubbles is also able to alleviate scaling formation on the membrane surface and delay the critical point of super saturation that leads to a major flux decline. These results were consistent with the membrane surface inspection by SEM, which showed that the least severe crystal deposition occurred in the original module incorporating bubbling.

Overall, the introduction of gas bubbles in the DCMD process not only mitigates the temperature polarization effect, but also enhances surface shear rate to postpone scaling formation on the membrane surface. It is beneficial to high concentration MD applications.

Acknowledgements

This research grant is supported by the Singapore National Research Foundation under its Environmental & Water Technologies Strategic Research Programme and administered by the Environment & Water Industry Programme Office (EWI) of the PUB (#0901-IRIS-02-03). We also acknowledge the funding support from Singapore Economic Development Board to Singapore Membrane Technology Centre.

Nomenclature

C	Overall mass transfer coefficient, $kg \cdot m^{-2}\ h^{-1}\ Pa^{-1}$
CPC	The concentration polarization coefficient
d_o	Outlet diameter of membrane fiber, mm
d_s	Housing diameter, mm
E_t	Tensile module, MPa
Gz	Graetz number, *Re Pr (D/L)*
h_f	Film heat transfer coefficients from feed side, $W \cdot m^{-2}\ K^{-1}$
h_m	Heat transfer coefficients of the membrane, $W \cdot m^{-2}\ K^{-1}$
h_p	Film heat transfer coefficients from permeate side, $W \cdot m^{-2}\ K^{-1}$
h_v	Latent heat of evaporation, $kJ \cdot kg^{-1}$
J	Permeate flux, $kg \cdot m^{-2}\ h^{-1}$
k	The boundary layer mass transfer coefficient, $m \cdot s^{-1}$
n	No. of fibers
Nu	Nusselt number
Q	Volume flowrate, $L \cdot min^{-1}$
Re	Reynold number, $d_h v\rho/\mu$
T_f	Bulk temperature of the feed, K
T_{fm}	Temperature at the membrane wall on the feed side, K
T_p	Bulk temperature of the permeate, K
TPC	The temperature polarization coefficient
T_{pm}	Temperature at the membrane wall on the permeate side, K
T_m	Temperature at the membrane wall, K

Greek letters

η	Thermal efficiency of the DCMD module
μ	Viscosity, $kg \cdot m^{-1}s^{-1}$
Φ	Flux enhancement ratio
ε	Porosity, %
δ_b	Strain at break, %

Suffix

f	Feed
fi	Inlet of the membrane module in the feed side
fm	Membrane wall in the feed side
fo	Outlet of the membrane module in the feed side
g	Gas
gas	DCMD process with gas bubbling
nogas	DCMD process without gas bubbling
p	Permeate
pi	Inlet of the membrane module in the permeate side
pm	Membrane wall in the permeate side
po	Outlet of the membrane module in the permeate side

References

[1] S. Kubota, et al., Experiments on seawater desalination by membrane distillation, Desalination 69 (1) (1988) 19–26.
[2] F. Banat, R. Jumah, M. Garaibeh, Exploitation of solar energy collected by solar stills for desalination by membrane distillation, Renew. Energy 25 (2) (2002) 293–305.
[3] K.W. Lawson, D.R. Lloyd, Membrane distillation, J. Membr. Sci. 124 (1) (1997) 1–25.
[4] K.W. Lawson, D.R. Lloyd, Membrane distillation. I. Module design and performance evaluation using vacuum membrane distillation, J. Membr. Sci. 120 (1) (1996) 111–121.
[5] A.M. Alklaibi, N. Lior, Membrane-distillation desalination: status and potential, Desalination 171 (2) (2005) 111–131.
[6] M.T. Chan, et al., Membrane distillation crystallization of concentrated salts—flux and crystal formation, J. Membr. Sci. 257 (1–2) (2005) 144–155.
[7] M.T. Chan, Membrane distillation crystallization, The University of New South Wales, Sydney, Australia, 2005.
[8] L. Martínez-Díez, M.I. Vázquez-González, Temperature and concentration polarization in membrane distillation of aqueous salt solutions, J. Membr. Sci. 156 (1999).
[9] V. Calabro, E. Drioli, Polarization phenomena in integrated reverse osmosis and membrane distillation for seawater desalination and waste water treatment, Desalination 108 (1–3) (1997) 81–82.
[10] R.W. Schofield, et al., Factors affecting flux in membrane distillation, Desalination 77 (1990) 279–294.
[11] R.W. Schofield, A.G. Fane, C.J.D. Fell, Heat and mass transfer in membrane distillation, J. Membr. Sci. 33 (3) (1987) 299–313.
[12] M.M. Teoh, S. Bonyadi, T.-S. Chung, Investigation of different hollow fiber module designs for flux enhancement in the membrane distillation process, J. Membr. Sci. 311 (1–2) (2008) 371–379.
[13] X. Yang, R. Wang, A.G. Fane, Novel designs for improving the performance of hollow fiber membrane distillation modules, J. Membr. Sci. 384 (1–2) (2011) 52–62.
[14] Z.F. Cui, S. Chang, A.G. Fane, The use of gas bubbling to enhance membrane processes, J. Membr. Sci. 221 (1–2) (2003) 1–35.
[15] F. Tajima, T. Yamamoto, Apparatus for filtering water containing radioactive substances in nuclear power plants. Toshiba, U.S. Patent 1988. 4.
[16] M. Mercier, C. Fonade, C. Lafforgue-Delorme, How slug flow can enhance the ultrafiltration flux in mineral tubular membranes, J. Membr. Sci. 128 (1) (1997) 103–113.

[17] C. Cabassud, S. Laborie, J.M. Lainé, How slug flow can improve ultrafiltration flux in organic hollow fibres, J. Membr. Sci. 128 (1) (1997) 93–101.
[18] Z.F. Cui, K.I.T. Wright, Gas—liquid two-phase cross-flow ultrafiltration of BSA and dextran solutions, J. Membr. Sci. 90 (1–2) (1994) 183–189.
[19] L. Vera, S. Delgado, S. Elmaleh, Dimensionless numbers for the steady-state flux of cross-flow microfiltration and ultrafiltration with gas sparging, Chem. Eng. Sci. 55 (17) (2000) 3419–3428.
[20] A.P.S. Yeo, A.W.K. Law, A.G. Fane, The relationship between performance of submerged
hollow fibers and bubble-induced phenomena examined by particle
image velocimetry, J. Membr. Sci. 304 (1–2) (2007) 125–137.
[21] A.P.S. Yeo, A.W.K. Law, A.G. Fane, Factors affecting the performance of a submerged hollow fiber bundle, J. Membr. Sci. 280 (1–2) (2006) 969–982.
[22] N. Ratkovich, et al., Experimental study and CFD modelling of a two-phase slug flow for an airlift tubular membrane, Chem. Eng. Sci. 64 (16) (2009) 3576–3584.
[23] S. Delgado, R. Villarroel, E. González, Effect of the shear intensity on fouling in submerged membrane bioreactor for wastewater treatment, J. Membr. Sci. 311 (1–2) (2008) 173–181.
[24] J. Phattaranawik, et al., A novel membrane bioreactor based on membrane distillation, Desalination 223 (1–3) (2008) 386–395.
[25] J. Zhang, et al., Performance of asymmetric hollow fibre membranes in membrane distillation under various configurations and vacuum enhancement, J. Membr. Sci. 362 (1–2) (2010) 517–528.
[26] X. Yang, et al., Performance improvement of PVDF hollow fiber-based membrane distillation process, J. Membr. Sci. 369 (1–2) (2011) 437–447.
[27] B.E. Short, Flow geometry and heat exchanger performance, Chem. Eng. Prog. 61 (7) (1965).
[28] R.H. Perry, D.W. Green, J.O. Maloney, Perry's chemical engineers' handbook, McGraw-Hill Companies, Inc., New York, 1997.
[29] H. Yu, et al., Numerical simulation of heat and mass transfer in direct membrane distillation in a hollow fiber module with laminar flow, J. Membr. Sci. 384 (1–2)(2011) 107–116

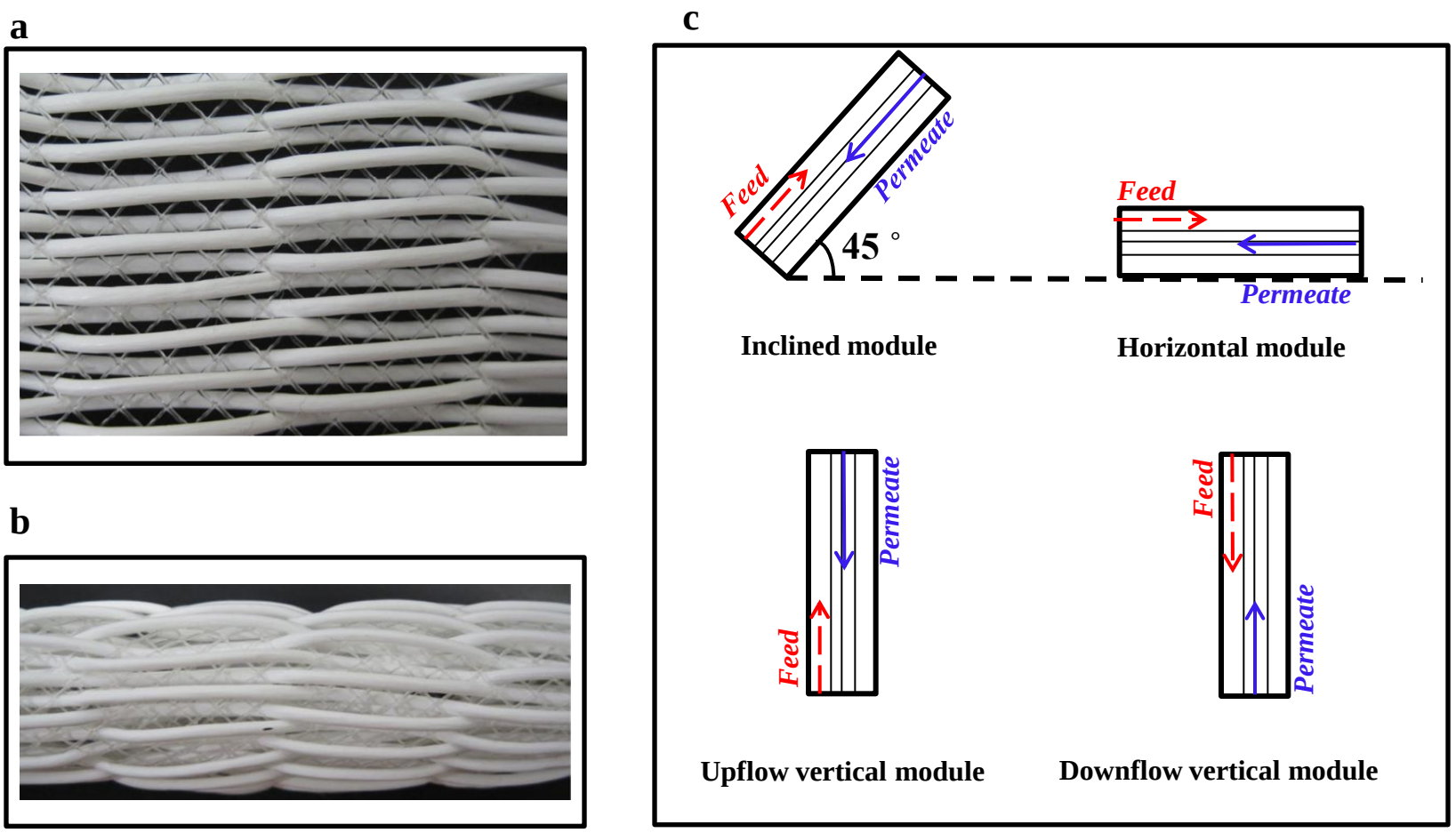

Figure 1. Several explanations for MD modules (a. Fibers knitted with spacers before packing; b. Hollow fibers in the membrane module after packing; c. Membrane module orientations).

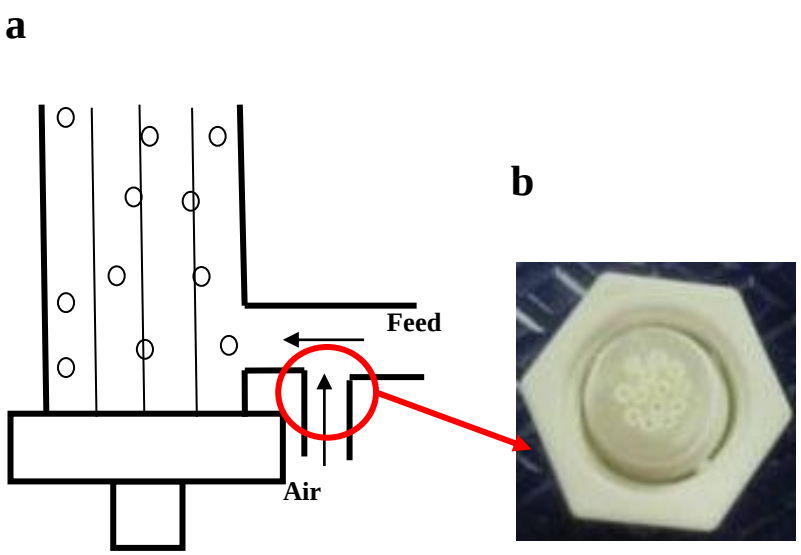

Figure 2. a. Air inlet connected to the membrane module; b. Air nozzle.

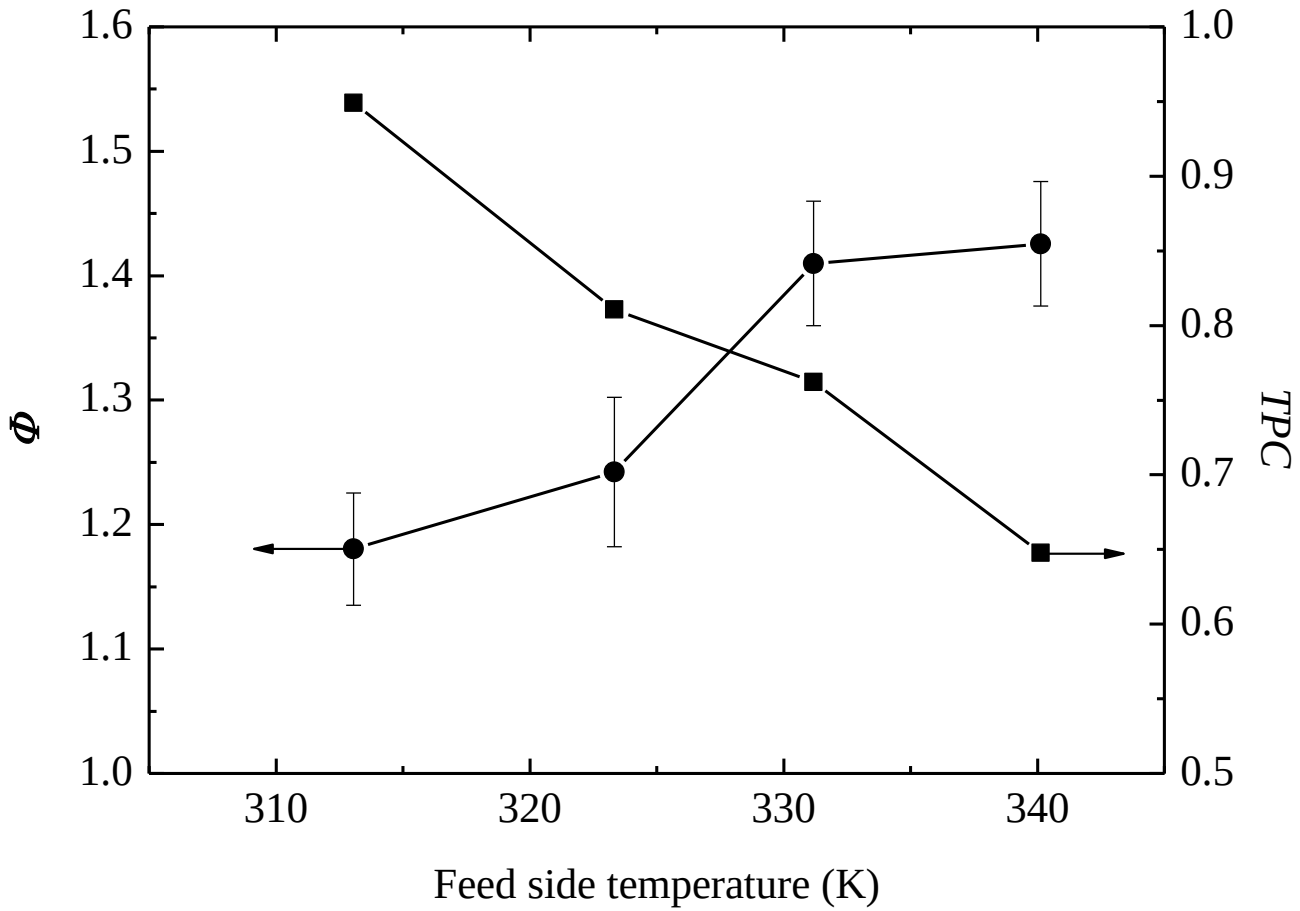

Figure 3. Effect of feed side temperature on Φ and *TPC*.
(3.5% NaCl solution as feed: Q_f = 0.3 L·min^{-1}; Q_p = 0.025 L·min^{-1} Q_g = 0.2 L·min^{-1}; T_p = 298 K)

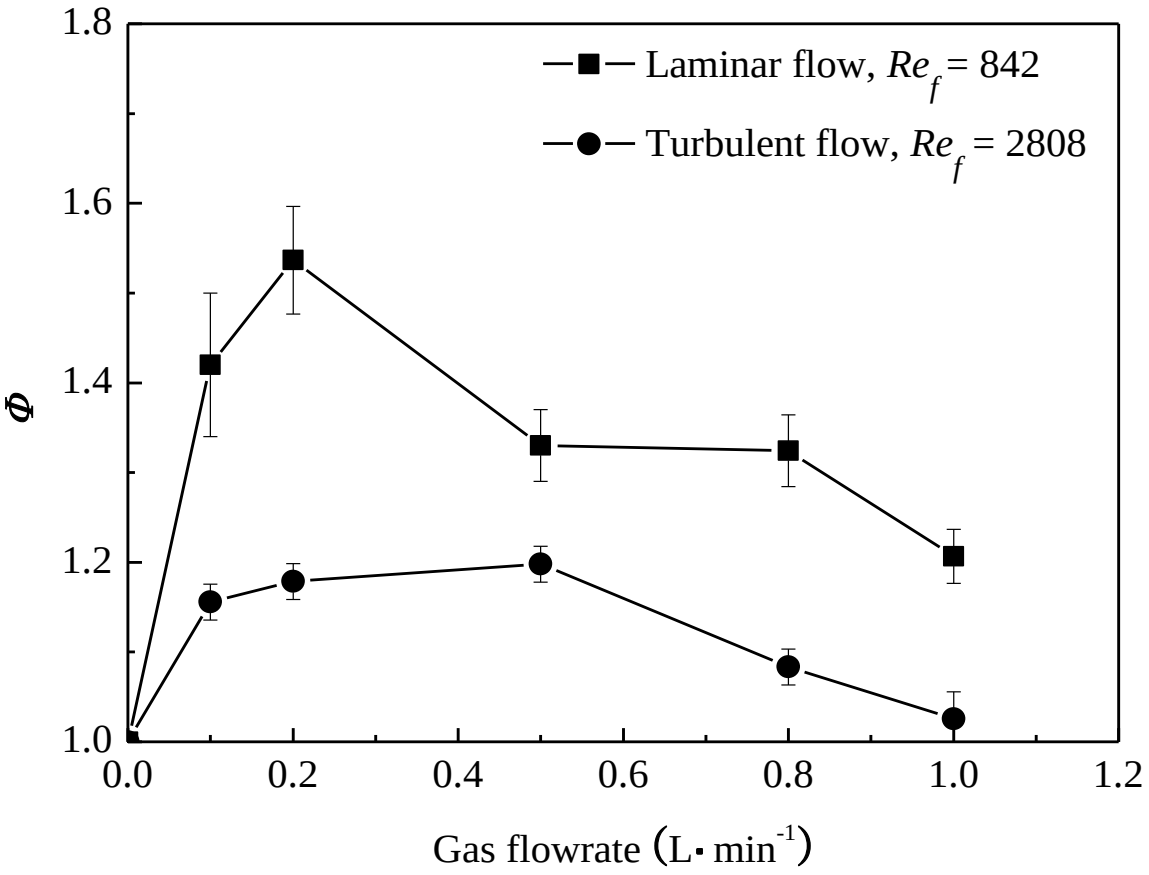

Figure 4. Effect of gas flowrate on Φ in laminar and turbulent flows. (3.5% NaCl solution as feed; Re_p = 552; T_f = 333 K; T_p = 298 K)

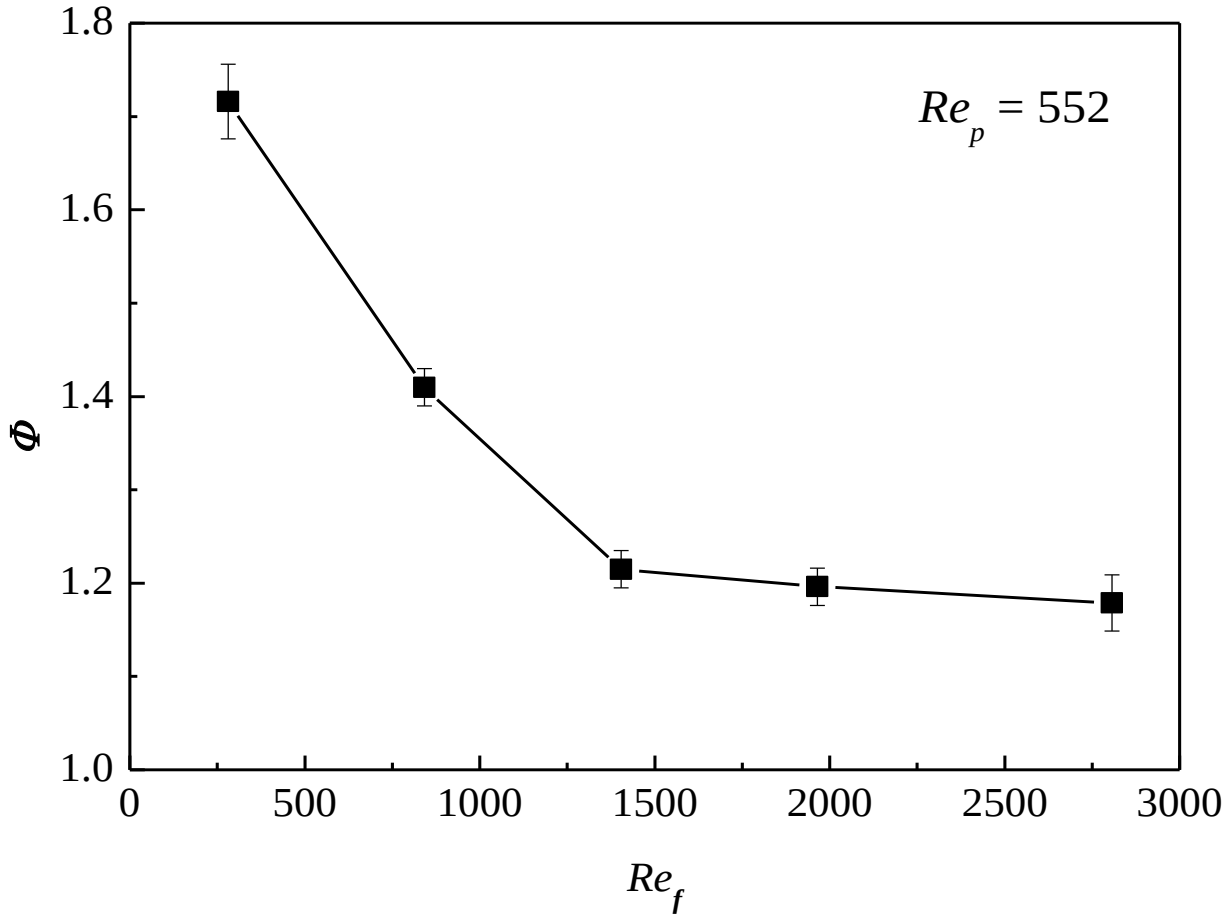

Figure 5. Effect of feed side Reynolds number on Φ.
(3.5% NaCl solution as feed; Q_g = 0.2 L·min^{-1}; T_f = 333 K; T_p = 298 K)

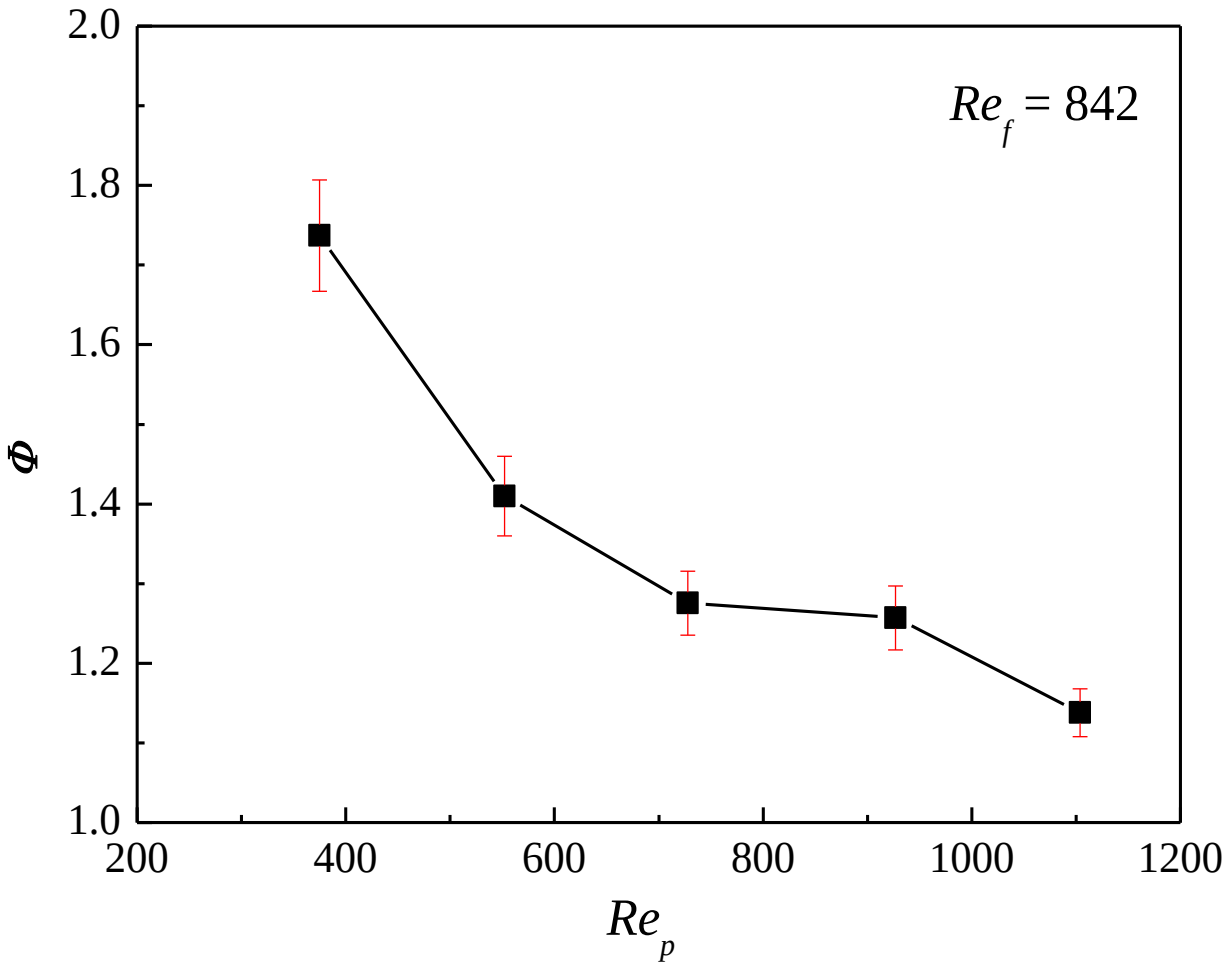

Figure 6. Effect of permeate side Reynolds number on Φ.
(3.5% NaCl solution as feed; Q_g = 0.2 L·min^{-1}; T_f = 333 K; T_p = 298 K)

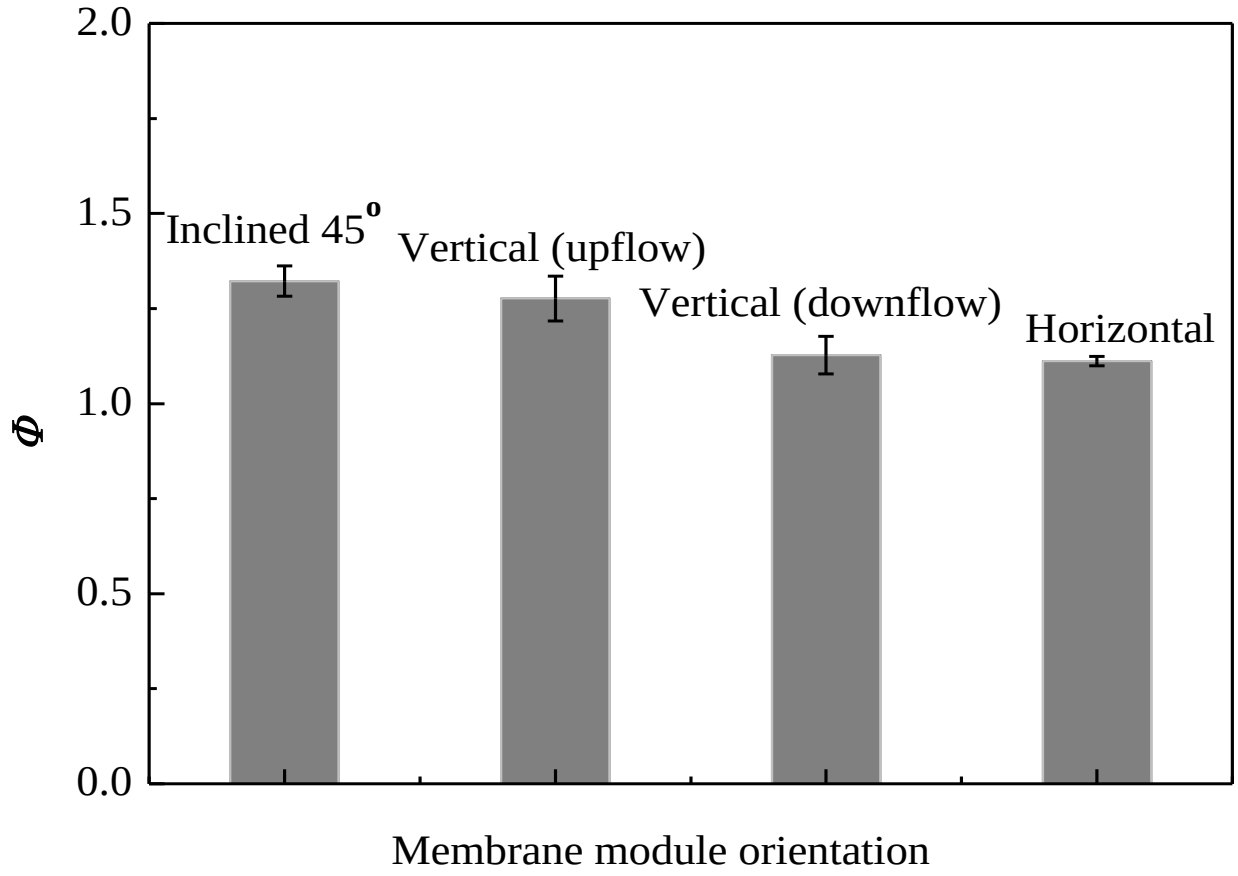

Figure 7. Effect of membrane module orientation on Φ.
(3.5% NaCl solution as feed: Q_f = 0.3 L·min^{-1}; Q_p = 0.025 L·min^{-1}; Q_g = 0.2 L·min^{-1}; T_f = 333 K; T_p = 298 K)

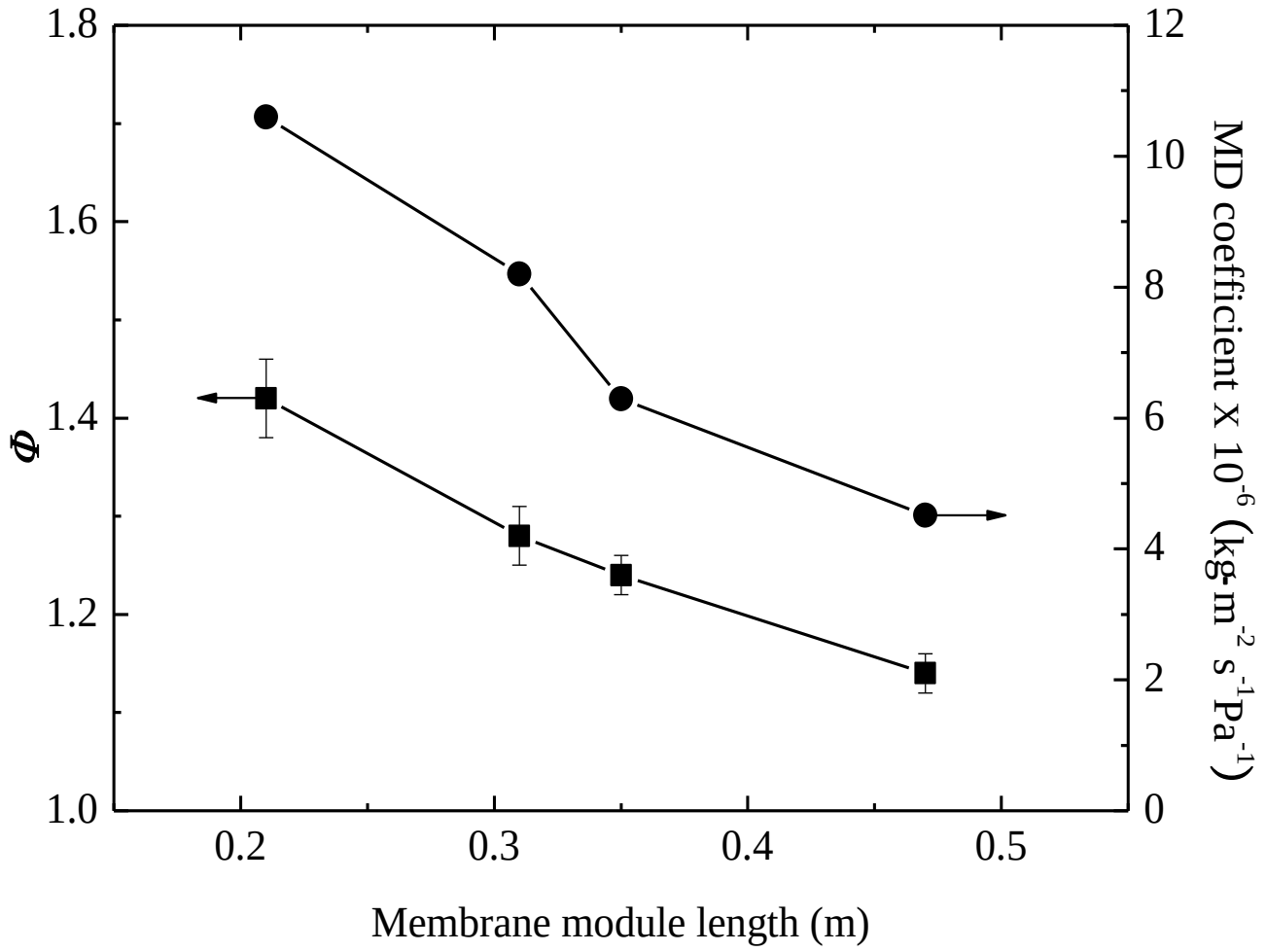

Figure 8. Effect of membrane module length on Φ.
(3.5% NaCl solution as feed: Q_f = 0.3 L·min^{-1}; Q_p = 0.025 L·min^{-1}; Q_g = 0.2 L·min^{-1}; T_f = 333 K; T_p = 298 K)

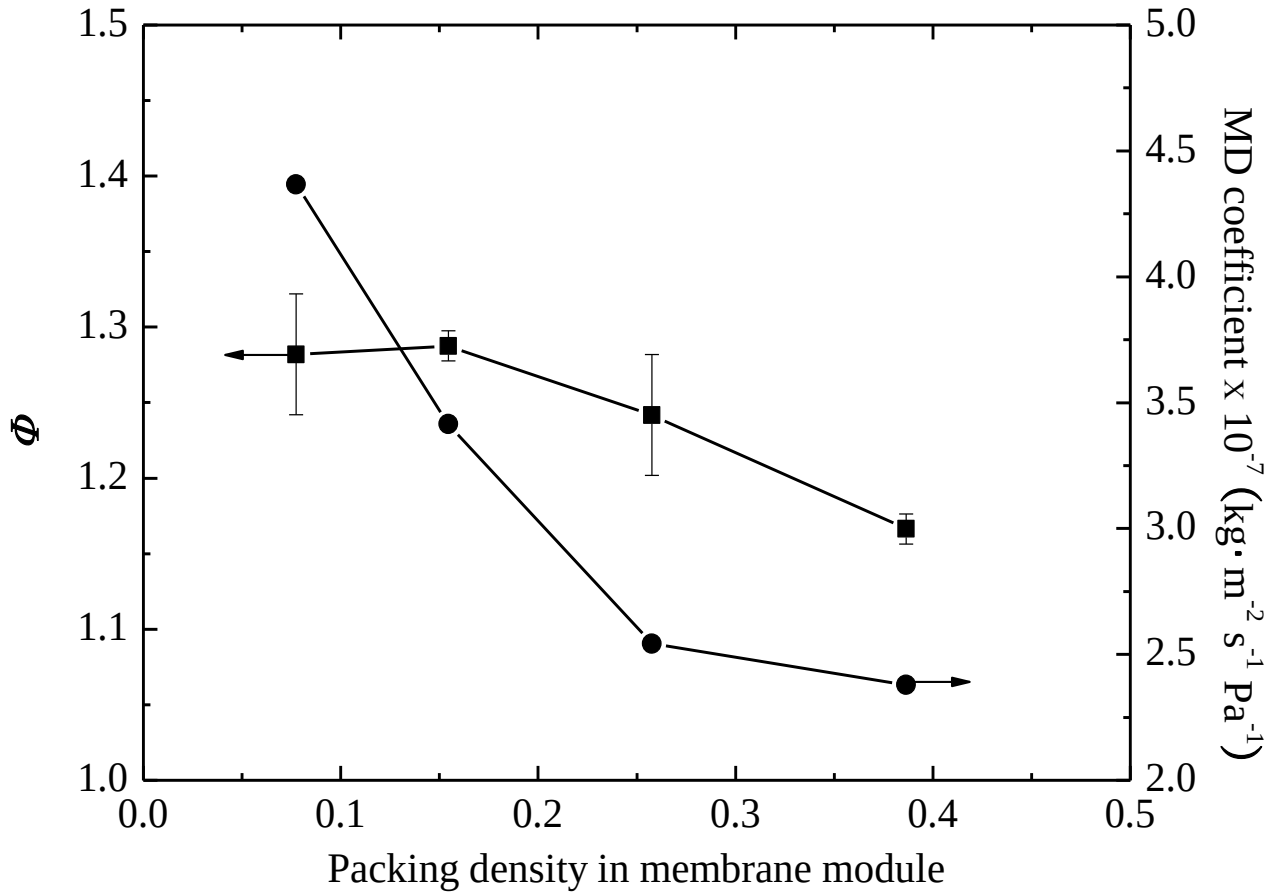

Figure 9. Effect of packing density in membrane module on Φ.
(3.5% NaCl solution as feed: Q_f = 0.3 L·min^{-1}; Q_p = 0.025 L·min^{-1}; Q_g = 0.2 L·min^{-1}; T_f = 333 K; T_p = 298 K)

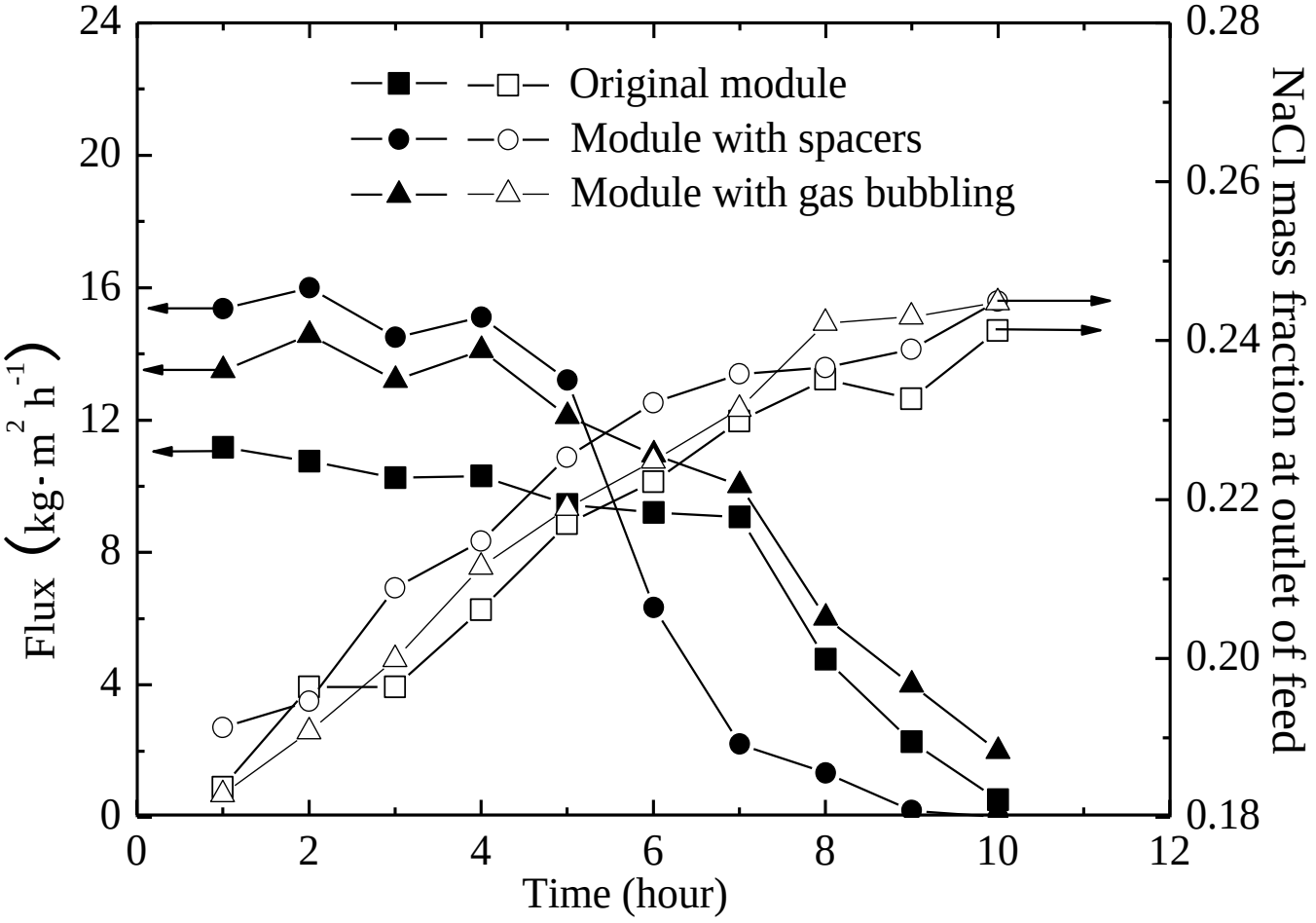

Figure 10. Flux and NaCl mass fraction at outlet of feed side vs time (Q_f = 0.6 L·min^{-1}; Q_p = 0.15 L·min^{-1}; Q_g = 0.2 L·min^{-1}; T_f = 333 K; T_p = 298 K; initial feed volume: 4000 ml)

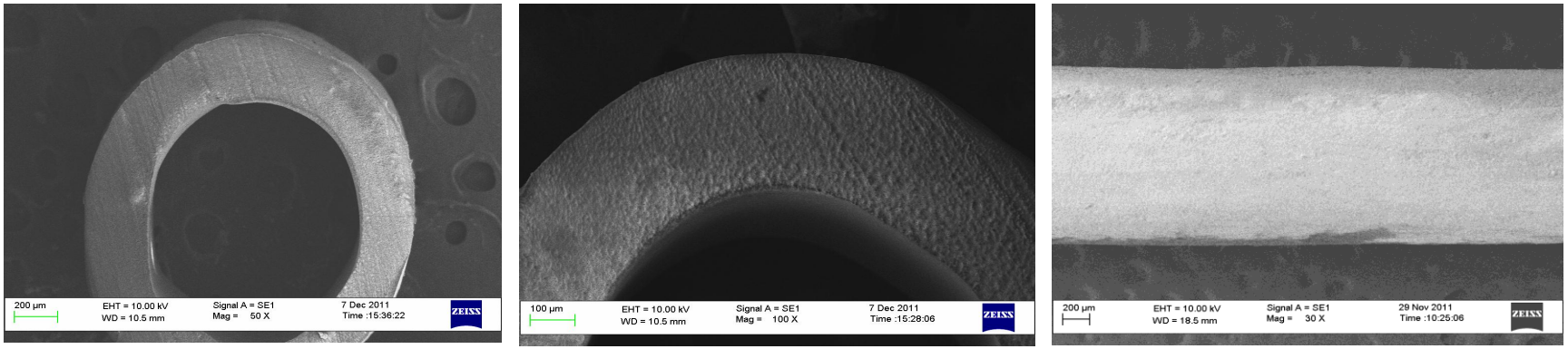

Figure 11(a). SEM images of cross section and membrane surface after 1 hour high concentration DCMD running

Original module

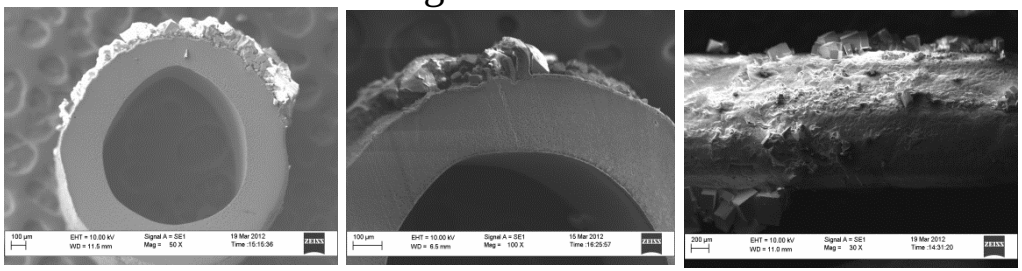

Module with bubbling

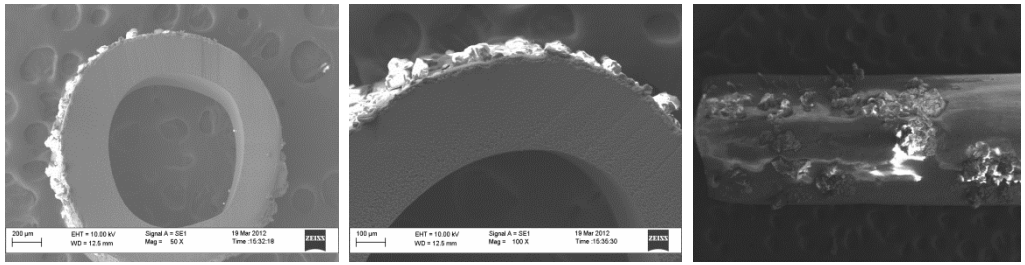

Module with spacers

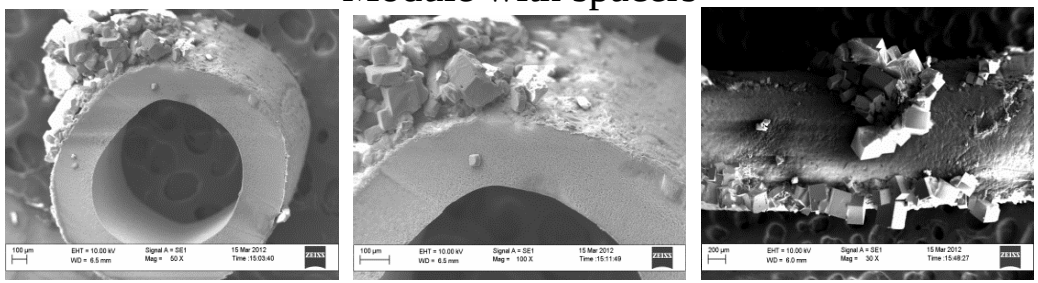

Figure 11(b). SEM images of cross section and membrane surface after 5 hours high concentration DCMD running

Original module

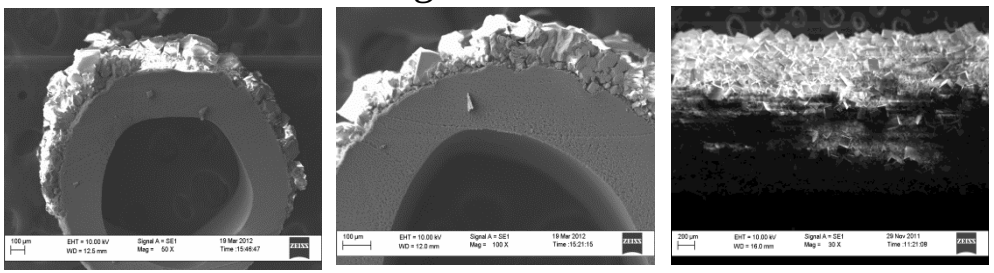

Module with bubbling

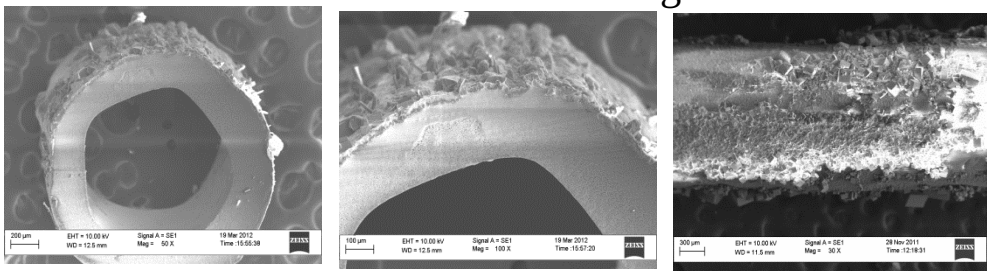

Module with spacers

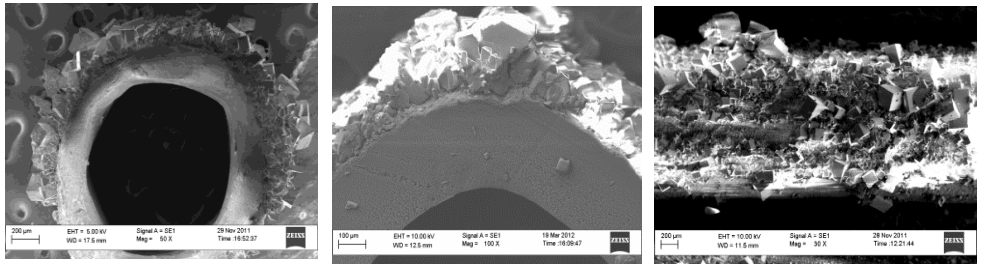

Figure 11(c). SEM images of cross section and membrane surface after 7 hours high concentration DCMD running

Table 1.PVDF membrane properties

Dimension	**Pore size (µm)**	**Contact angle (˚)**	**Porosity ε (%)**	**LEPw (bar)**	**Tensile module E_t (MPa)**	**Strain at break δ_b (%)**
d_o: 1.525mm δ_m: 206.8 µm	r_{max}: 0.125 r_{mean}: 0.082	106-120	82-85	3.5	42.05	10.5

Table 2. Membrane module specifications

Experiment type	**Housing diameter, d_s(mm)**	**No. of fibers, *n***	**Effective fiber length, *L*(mm)**	**Packing density, (%)**	**Membrane area, *A*(m^2)**
Module #1	6	1-6	210-480	8-49	0.001-0.006
Module #2 & #3	9.5	6	340	26	0.0098